THEORETICAL & APPLIED MECHANICS LETTERS **1**, 012001 (2011)

Numerical simulation of multiphase cavitating flows around an underwater projectile

Jian-hong Guo,[1, a)] Chuan-jing Lu,[1,2, b)] and Ying Chen[1]
[1)] *School of Naval Architecture, Ocean and Civil Engineering, Shanghai Jiaotong University, Shanghai 200240*
[2)] *State Key Laboratory of Ocean Engineering, Shanghai 200030*

(Received 5 September 2010; accepted 28 November 2010; published online 10 January 2011)

Abstract The present simulation investigates the multiphase cavitating flow around an underwater projectile. Based on the Homogeneous Equilibrium Flow assumption, a mixture model is applied to simulate the multiphase cavitating flow including ventilated cavitation caused by air injection as well as natural cavitation that forms in a region where the pressure of liquid falls below its vapor pressure. The transport equation cavitating model is applied. The calculations are executed based on a suite of CFD code. The hydrodynamics characteristics of flow field under the interaction of natural cavitation and ventilated cavitation is analyzed. The results indicate that the ventilated cavitation number is under a combined effect of the natural cavitation number and gas flow rate in the multiphase cavitating flows. © *2011 The Chinese Society of Theoretical and Applied Mechanics.* [doi:10.1063/2.1101201]

Keywords multiphase flow, natural cavitation, ventilated cavitation, projectile

It is encouraging to recognize that the drag will reduce greatly if an underwater projectile is enveloped in a supercavity. For engineering applications of supercavitation technique, it is necessary to keep the cavitation number within a favorable range and ventilation looks to be the most promising tool for control of supercavitating flows. In general, high-speed supercavitating vehicles are designed with ventilation ports at or near the cavitator leading edge, where natural (vapor) cavitation will likely also occur when the pressure decreases to below the vapor pressure. As a result, the flow field will become so complex with respect to mass transfer because of phase change as well as the transportation of momentum, energy among liquid and vapor and gas phase. In addition, the interaction of vapor cavitation and injected gas may cause a change of phase content in the cavity and hydrodynamic characteristic of the flow field. The physical properties of such flow are highly nonlinear and remain only partially understood. Previously, Kunz[1] *et al.* have numerically made three-dimensional analysis of a notional vehicle with natural cavitation, non-condensable gas injection and propulsion stream to illustrate the three-species nature of the model and formulation. Yuan[2] investigated the strong interaction between internal cavitating flow and external jet flow of injection nozzles and indicated the potential of cavitation for enhancement of atomization and spray quality. Feng[3,4] *et al.* had once investigated the characteristics of hydrodynamic forces for cavities with and without ventilation, they observed that the appearance of cavities due to ventilation changed especially in the wake of the cavity and the drag coefficient showed the decreasing trend under ventilation condition. Owis[5] simulated the bubble shape over a hemispherical body with gas injection and natural cavitation, and concluded that the viscous drag was significantly reduced due to gas injection on the body nose.

It should be noted that the experiments on multiphase cavitating flows at the relatively small natural cavitation number are scarce. Moreover, most existing experimental studies could not provide the details of the phase structure inside the cavity due to the difficulty in distinguishing vapor and non-condensable gas. In this paper numerical approaches are applied to model the multiphase cavitating flows. The main motivation is to study the shape and internal structure of cavities filled with vapor, non-condensable gas and liquid, to analyze the interaction between vapor cavities and ventilated cavities at the relatively small natural cavitation numbers.

A model for multiphase turbulent cavitating flow considering the liquid, vapor, non-condensable gas is applied. The baseline governing differential system includes the mass conservation equation and Reynolds-Averaged Navier–Stokes equation

$$\frac{\partial \rho}{\partial t} + \nabla \cdot (\rho \boldsymbol{V}) = 0, \tag{1}$$

$$\frac{\partial (\rho \boldsymbol{V})}{\partial t} + \nabla \cdot (\rho \boldsymbol{V}\boldsymbol{V}) = \nabla \left(p + \frac{2}{3}\mu_{\mathrm{e}} \nabla \cdot \boldsymbol{V} \right) - \nabla \cdot (\mu_{\mathrm{e}} \boldsymbol{S}) + \rho \boldsymbol{g}, \tag{2}$$

where $\boldsymbol{V}$ is the velocity vector, $\boldsymbol{S}$ is the rate of deformation tensor, $\boldsymbol{g}$ is the gravitational acceleration, p is the dynamic pressure. The effective viscosity μ_{e} is defined as the sum of molecular viscosity μ and turbulent viscosity μ_{t}.

Based on the turbulent viscosity hypothesis, a local linear low-Reynolds-number modified k-ε turbulence model[5] is applied here.

A transport equation cavitation model is used. Firstly, we define the phase mass fraction f_i, the phase

[a)] E-mail: guojh8011@gmail.com
[b)] Corresponding author. E-mail: cjlu@sjtu.edu.cn

volume fraction α_i, the phase density ρ_i, the phase molecular viscosity μ_i, where the subscripts i=l, v, g denote liquid, vapor and non-condensable phase respectively. In this model, the vapor mass fraction f_v and the gas mass fraction f_g transport equations are solved, where the liquid mass fraction can be obtained by $f_\mathrm{l} = 1 - f_\mathrm{g} - f_\mathrm{v}$. Phase transition processes are simulated by means of a physical rate[7] that appears in the right side of the vapor mass fraction equation (3) as a source term.

$$\frac{\partial(\rho f_\mathrm{v})}{\partial t} + \nabla\cdot(\rho \boldsymbol{V} f_\mathrm{v}) = \left(\dot{m}^- - \dot{m}^+\right), \tag{3}$$

$$\frac{\partial(\rho f_\mathrm{g})}{\partial t} + \nabla\cdot(\rho \boldsymbol{V} f_\mathrm{g}) = 0, \tag{4}$$

where $(\dot{m}^- - \dot{m}^+)$ is the net phase change rate. $\dot{m}^-$ is the mass transfer rate from liquid to vapor

$$\dot{m}^- = c_\mathrm{e}\frac{\sqrt{k}}{\sigma}\rho_\mathrm{l}\rho_\mathrm{v}\left(\frac{2}{3}\frac{p_\mathrm{v}-p}{\rho_\mathrm{l}}\right)^{1/2}(1-f_\mathrm{v}-f_\mathrm{g}), \tag{5}$$

$\dot{m}^+$ is the mass transfer rate from vapor to liquid

$$\dot{m}^+ = c_\mathrm{c}\frac{\sqrt{k}}{\sigma}\rho_\mathrm{l}\rho_\mathrm{l}\left(\frac{2}{3}\frac{p-p_\mathrm{v}}{\rho_\mathrm{l}}\right)^{1/2} f_\mathrm{v}, \tag{6}$$

where the values of empirical constants c_e and c_c, which regulate the rate of evaporation and condensation of phases respectively, are 0.02 and 0.01, surface tension σ to 0.717 N/m.

The phase volume fraction can be calculated by

$$\alpha_i = f_i\rho/\rho_i. \tag{7}$$

Then the mixture density and the mixture dynamic viscosity are calculated as

$$\frac{1}{\rho} = \frac{f_\mathrm{v}}{\rho_\mathrm{v}} + \frac{f_\mathrm{g}}{\rho_\mathrm{g}} + \frac{1-f_\mathrm{v}-f_\mathrm{g}}{\rho_\mathrm{l}}, \tag{8}$$

$$\mu = \alpha_\mathrm{l}\mu_\mathrm{l} + \alpha_\mathrm{v}\mu_\mathrm{v} + \alpha_\mathrm{g}\mu_\mathrm{g}. \tag{9}$$

The calculations are executed on a suite of CFD code which is evolved from works of Xue,[8] Wu[9] and Chen[10] and is developed further here. A sketch of the computational model, boundary condition, arrangement of ventilated ports and grid distribution at the head of the projectile is schematically represented in Fig 1. The diameter of projectile D is 76 mm and the diameter of disk cavitator D_n equates to 20%D. An eight-block structured grid is used composed of 128 660 cells and clustered tightly to the wall and to the region where cavitation is expected. In all the cases, gas is injected normal to the port surface.

In the simulations, different boundary conditions are used including inlet, outlet and no-slip wall boundary conditions. At the inlet, the velocity, the phase

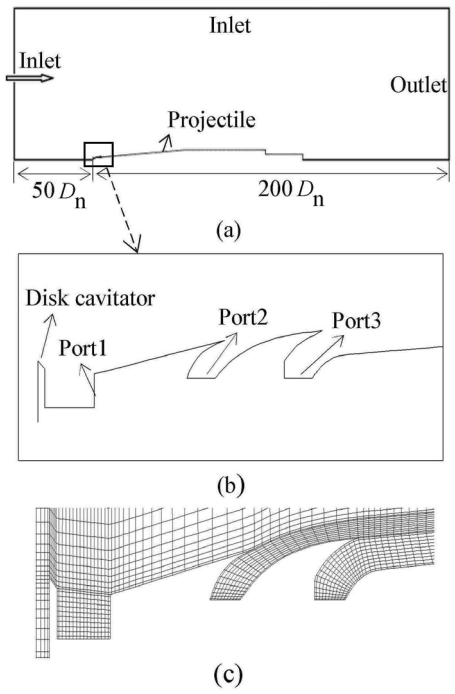

Fig. 1. (a) Computational model and boundary condition; (b) location of three ventilation ports; (c) grid distribution near the head of projectile.

mass fractions and the turbulence variables are specified, whereas the pressure is extrapolated from the interior points; at the outlet, all the variables are extrapolated from the interior points; and at the no-slip walls, the velocities are set equal to zero, whereas the pressure, the turbulence variables and the mass fractions are extrapolated from the interior points.

The characteristic parameters are defined as

$$\sigma_\mathrm{v} = \frac{2(p_\infty - p_\mathrm{v})}{\rho_\mathrm{l}u_\infty^2},\ \sigma_\mathrm{c} = \frac{2(p_\infty - p_\mathrm{c})}{\rho_\mathrm{l}u_\infty^2},$$
$$c_\mathrm{Qv} = \frac{Q}{u_\infty A},\ Re = \frac{\rho_\mathrm{l}u_\infty D}{\mu_\mathrm{l}},\ C_\mathrm{d} = \frac{F_D}{1/2\rho_\mathrm{l}u_\infty^2 A}, \tag{10}$$

where σ_v is the natural cavitation number, σ_c is the ventilated cavitation number, c_Qv is the volumetric flow rate coefficient, p_∞ is the pressure at infinity, u_∞ is the inflow velocity, p_v is the saturation vapor pressure, p_c is the pressure in the cavity, Q is the volumetric flow rate at one atmospheric pressure, A is the maximum cross-sectional area of the body and F_D is the total drag.

Firstly, two cases are computed at $\sigma_\mathrm{v} = 0.04$. In the first case, natural cavitation without gas injection is simulated. In the second case, a certain amount of non-condensable gas is injected into the flow field from port 2 and port 3 when port 1 is closed. Figures 2 and 3 show the cavity shapes of natural and ventilated cavities at the same cavitation number, that is the natural cavitation number for the natural cavitating flow and refers to the ventilated cavitation number for the mul-

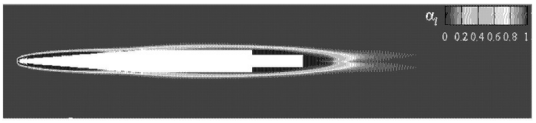

Fig. 2. Water volume fractions for the natural cavity, $\sigma_v = 0.04$.

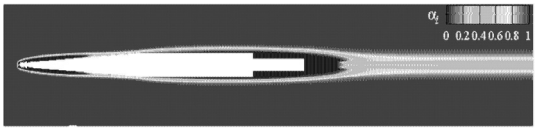

Fig. 3. Water volume fractions for the ventilated cavity, $\sigma_c = 0.0404$, $c_{Qv} = 0.109$.

tiphase cavitating flow. For both cases, the projectile is enveloped by two partial cavities, where the first one is excited by the disk cavitator mounted at the head of the projectile and the other one extends from the shoulder of the projectile to the wake. The comparison of cavity shapes shown in Figs. 2 and 3 indicates that the first partial cavity in the ventilated cavitating flow becomes shorter than that in the natural cavitating flow, whereas the tail of the second partial cavity grows thicker in the ventilated cavitating flow. In the wake of the cavitating flow, the rear of the ventilated cavity has gas leakage continuously while the rear of the natural cavity is closed by a re-entrant jet. The time variations of the drag coefficient for the both cases are shown in Fig.4. It can be seen that the drag becomes lower in the ventilated cavitating flow than that in the natural cavitating flow. The reason is that the wetted area decreases when the region between the two partial cavities is covered by a thin layer of gas–water mixture as gas is injected into the flow field.

In order to study the influence of in-flow conditions on the characteristics of multiphase cavities, two sets of calculations were carried out for the cases with $Re = 7.56 \times 10^5$, $\sigma_v = 0.03$ and $Re = 7.56 \times 10^5$, $\sigma_v = 0.08$ at the different gas flow rate. In the above cases, gas is injected into the cavities through all the ports.

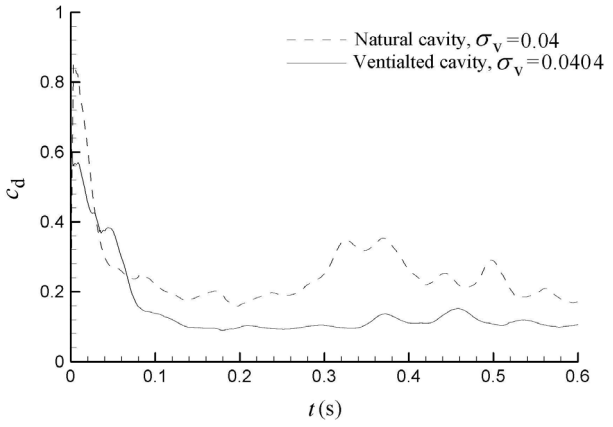

Fig. 4. Time variation of the drag coefficient for the cavitating flows without and with gas injection.

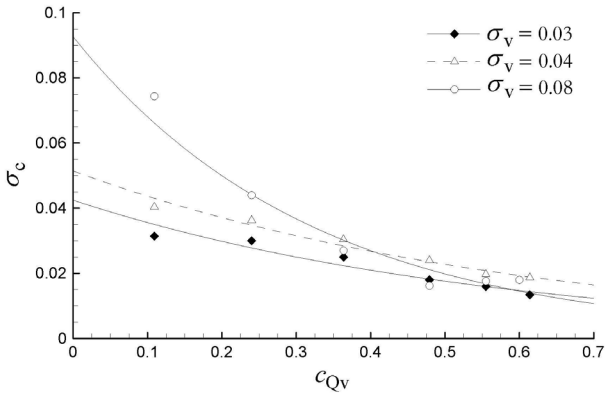

Fig. 5. The variation of ventilated cavitation number with gas flow rate coefficient at the various values of σ_v.

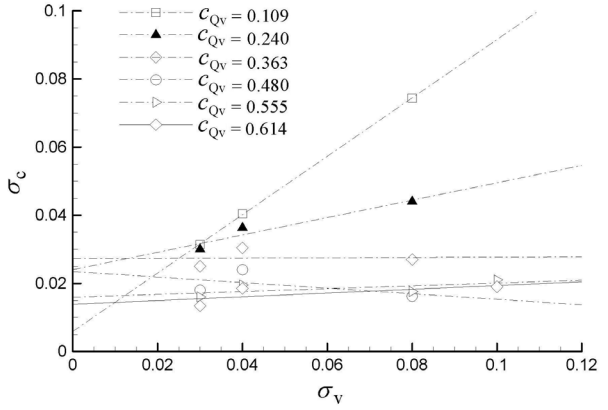

Fig. 6. The relationship between σ_c and σ_v.

Figure 5 shows the relationship between the ventilated cavitation numbers and the volume gas flow rates at the various natural cavitation numbers. Note that the ventilated cavitation numbers at the large natural cavitation numbers have a steep decrease with the increase of gas flow rates. This plot shows also that the ventilated cavitation numbers at the small gas flow rate are greatly related to the natural cavitation numbers. However, once the gas flow rate increases to a certain value, the ventilated cavitation numbers depend mainly on the gas flow rates, but have little relationship with the natural cavitation number which suggests that the cavities are mostly filled with gas.

Figure 6 shows the relationship between ventilated cavitation numbers and the natural cavitation numbers at the different gas flow rates. It can be seen that the ventilated cavitation numbers hardly depend on the natural cavitation numbers as the gas supply is large enough. It means that the natural cavitation will be repressed as the gas supply increases to a certain value. As shown in Fig. 7, the drag coefficient is also hardly

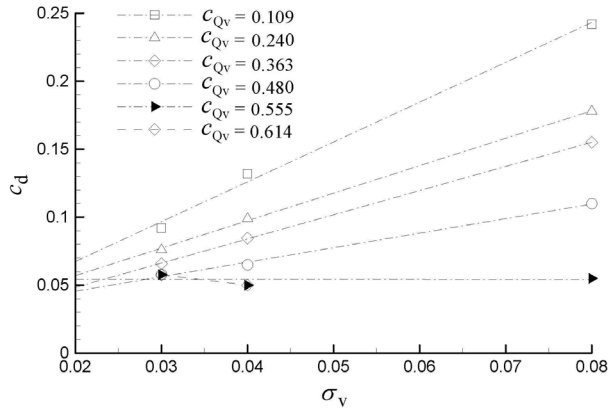

Fig. 7. The variation of drag coefficient with σ_v at the different gas flow rate.

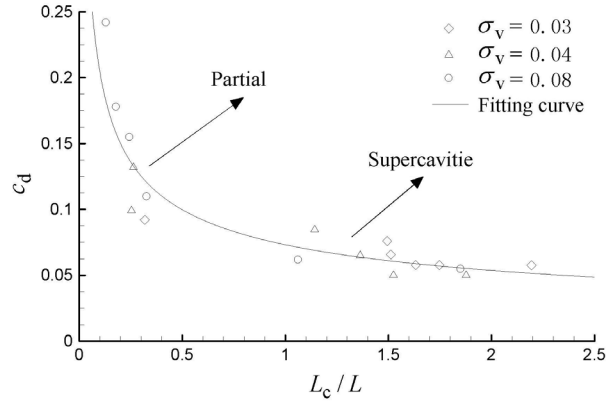

Fig. 8. Drag coefficient versus cavity length.

influenced by the natural cavitation numbers as the gas flow rate is greater than 0.555. It means that the cavities are mostly filled with the injected air as the gas supply is large enough.

The drag coefficient is related closely to the cavity dimension. Figure 8 gives the calculated results of the relationship between the non-dimensional cavity length and drag coefficient, where L_c is the cavity length, L is the length of the projectile. When the cavity length extends beyond the length of the body, the drag coefficient undergoes an abrupt reduction.

From the simulation on the multiphase cavitating flows over an underwater projectile, some basic characteristics of flow field and hydrodynamics are found. The main conclusions are summarized as follows:

(1) The morphology of multiphase cavities is similar to that of natural cavities at the same cavitation number except the tail of the cavity where gas escapes from the cavity continuously, while the rear of the natural cavity is closed by a re-entrant jet.

(2) The drag coefficient under a ventilation condition tends to decrease compared to that of fully natural cavity at the same cavitation number.

(3) In the multiphase cavitating flows, the ventilated cavitation numbers are under a combined effect of the natural cavitation numbers and gas flow rates.

Though the model used here can be applied to a wide range of geometric systems and problems, there are certain limitations for the cavitation model including the use of experience parameters in the phase change rate in Eq. (3), and ignoring the thermal effect in the cavitation process. The further efforts are expected to extend and improve the model.

The work was supported by the National Natural Science Foundation of China (Grant No:10832007) and Shanghai Leading Academic Discipline Project (Project No. B206).

1. R. F. Kunz, J. W. Lindau, L. B. Michael, and R. S. David, VKI Special Course on Supercavitating Flows, February 12-16 2001 in Brussels, Belgium (2001).
2. W. Yuan and G. H. Schnerr, J. Fluids Engineering, **125**, 963 (2003).
3. X. M. FENG, C. J. Lu, and T. Q. Hu, J. Hydrodynamics, Ser. B, **14**, 17 (2002).
4. X. M. Feng, C. J. Lu, T. Q. Hu, L. Wu, and J. Li, J. Hydrodynamics, Ser. B, **17**, 87 (2005).
5. M. O. Farouk and H. Na. Ali, European J. Mechanics B/Fluids. **23**, 339 (2004).
6. W. P. Jones and B. E. Launder, Int. J. Heat and Mass Transfer, **16**, 1119 (1973).
7. A. K. Singhal, M. M. Athavale, H. Y. Li, and Y. Jiang, J. Fluids Engineering, **124**, 617 (2002).
8. L. P. Xue, Entwicklung eines effizienten parallelen Lösungsalgorithmus zur dreidimensionalen Simulation komplexer turbulenter Strömungen, Ph. D. thesis, Technischen Universität Berlin, (1998).
9. L. Wu, C. J. Lu, J. Li, and X. Chen, J. Hydrodynamics, Ser.B, **18**, 341 (2006).
10. Y. Chen and C. J. Lu, J. Hydrodynamics, Ser. B, **20**, 186 (2008).